Equilibrium properties of a Josephson-junction ladder with screening effects

Juan J. Mazo
Departamento de Física de la Materia Condensada and Instituto de Ciencia de Materiales de Aragón, Consejo Superior de Investigaciones Científicas, Universidad de Zaragoza, 50009 Zaragoza, Spain and Dipartimento di Fisica. Università di Roma Tor Vergata, Via della Ricerca Scientifica 1, 00133 Roma, Italy

José C. Ciria
Dipartimento di Fisica, Università di Roma Tor Vergata, Via della Ricerca Scientifica 1, 00133 Roma, Italy
(Received 29 February 1996)

We calculate the ground-state phase diagram of a Josephson-junction ladder when screening field effects are taken into account. We study the ground-state configuration as a function of the external field, the penetration depth, and the anisotropy of the ladder, using different approximations to the calculation of the induced fields. A series of tongues, characterized by the vortex density ω, is obtained. The vortex density of the ground state, as a function of the external field, is a devil's staircase, with a plateau for every rational value of ω. The width of each of these steps depends strongly on the approximation made when calculating the inductance effect: If the self-inductance matrix is considered, the $\omega=0$ phase tends to occupy all the diagram as the penetration depth decreases. If, instead, the whole inductance matrix is considered, the width of any step tends to a nonzero value in the limit of very low penetration depth. We have also analyzed the stability of some simple metastable phases: Screening fields are shown to enlarge their stability range. [S0163-1829(96)06046-8]

I. INTRODUCTION

Theoretical research in Josephson-junction arrays (JJA's) is continuously progressing through models which involve increasing complexity. They represent a better approximation to the understanding and prediction of the many different interesting phenomena which occur in such systems.[1] An important contribution to this advance is the inclusion of current-induced magnetic fields (CIMF's) developed by different groups in the last years.[2] Taking CIMF's into account is compulsory in order to provide a correct description of Josephson-junction arrays at low temperature, when the penetration depth of the magnetic field is of about the cell size.

In all the cases, the study was carried out through the numerical simulation of the dynamics of the gauge-invariant phase differences. Interest has been mainly focused on the effects of CIMF's in the properties of arrays driven by external currents. However, we have no knowledge of studies on the ground-state properties of inductive arrays.

This paper deals with the static properties of a Josephson-junction ladder (JJL), with anisotropy in the Josephson couplings, in the presence of an external magnetic field (Fig. 1). In particular, we have calculated the ground-state phase diagram of a system defined by a Hamiltonian which includes the magnetic energy due to the CIMF's, in addition to the usual Josephson coupling contribution.

Recently two different groups[3,4] have faced the ground-state problem of a JJL in the presence of a magnetic field and in the limit of infinite penetration depth: no screening effects. In this approximation, some general properties concerning the ground states can be deduced. In regard to the ground-state problem, the Hamiltonian describing the system belongs to a universality class of convex one-dimensional (1D) models of spatially modulated structures,[3] such as the Frenkel-Kontorova model.[5] This fact allows an exact description of the ground-state phase diagram and the relevant elementary excitations of the system.[3] The diagram, a function of the external field and the anisotropy parameter, consists of a series of tongues labeled by the vortex density ω. Both rational and irrational values of ω are possible, corresponding, respectively, to commensurate and incommensurate phase configurations. The vortex density of ground-state configurations as a function of the external magnetic field is a devil's staircase function, with plateaus for every rational value of ω. Incommensurate ground states exhibit two regimes, separated by an Aubry transition:[6] Below a certain value of the parameter that describes the anisotropy, the configuration is undefectible (no defects can be sustained) and unpinned (any external current, though infinitesimal, causes

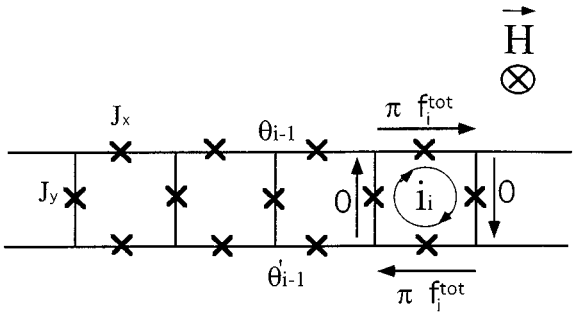

FIG. 1. Schematic representation of the Josephson-junction array we study here: an anisotropic ($J_x \neq J_y$) ladder, in the presence of an external field. The sites denote superconducting islands and the crosses the junctions themselves. The rightmost plaquette shows the mesh current i_i and the gauge choice, here $f_i^{\rm tot}=f_0+f_i$, where $f_0=Ha^2/\Phi_0$ is the flux due to the external field and f_i the induced flux in the plaquette i.

a nonzero voltage); above this value, the solution is defectible and pinned.

In this paper we use the work by Mazo *et al.*[3] as a starting point and include CIMF's. We thus obtain a more realistic description of the ground states and, in general, of the equilibrium properties of the ladder. Such results may be of interest in understanding experiments in JJL's where relevant parameters can be fixed at will.

We have used different numerical methods — effective potentials method combined with root-finding methods and stability analysis of solutions, as well as dynamical relaxation — in order to find the ground-state phase diagram and other metastable configurations. Results are obtained for three approximations to the calculation of the induced fields: (A) self-inductance contributions, (B) self-inductance plus nearest-neighbors mutual inductance contributions, and (C) full-inductance matrix. In all the cases the vortex density of the ground state, as a function of the external field, exhibits a devil's staircase structure. Special attention has been focused on the behavior of the system in the small penetration depth limit. In this limit, a vortex can be described as a flux quantum concentrated in one only cell. The ground-state phase diagram shows an important difference depending on the approximation made when calculating the inductance effect: If the self-inductance matrix is considered, the $\omega=0$ phase, in this limit, nearly occupies all the diagram. When the whole inductance matrix is considered we find ground states with no null vortex density in a wide region of the phase diagram.

The variation of the induced flux with the penetration depth allows an estimation of the physically interesting range of values of this array parameter. We have also studied the dependence of some of the vortex properties with the penetration depth and the anisotropy of the ladder, such as its extension and the distribution of gauge-invariant phases and the induced flux. Finally, we consider the stability of some simple metastable commensurate phases when the external field is varied. Notably, the stability intervals enlarge when the penetration depth decreases. There is a critical value of the penetration depth for the stability of each phase at zero external field.

The paper is organized as follows: In Sec. II we introduce the model and the different methods and approximations used to compute its properties. Results on the ground-state phase diagram and the stability of some simple commensurate phases are reported in Sec. III. Different approximations to the calculation of the CIMF's are discussed.

II. DESCRIPTION OF THE MODEL AND THE METHOD

The classical Hamiltonian[7] describing the system is

$$H=-\sum_i \left[J_x\cos(\theta_i-\theta_{i+1}-\pi f_0-\pi f_i) + J_x\cos(\theta_i'-\theta_{i+1}'+\pi f_0+\pi f_i) + J_y\cos(\theta_i-\theta_i')\right]+\frac{1}{2}\Phi_0^2\sum_{ij} f_i L_{ij}^{-1} f_j . \quad (1)$$

Here θ_i (θ_i') denotes the phase of the superconducting order parameter on the upper (lower) branch of the ladder at the ith site (see Fig. 1). f_0 is the magnetic flux due to the external field, which is assumed to be constant along the array. f_i is the induced flux through plaquette i, a function of the currents in the ladder. Both f_0 and f_i are expressed in terms of the flux quantum Φ_0. Thus, the total magnetic flux $\Phi_i^{\rm tot}$ through a given plaquette i is $\Phi_i^{\rm tot}=\Phi^{\rm ext}+\Phi_i^{\rm ind}=\Phi_0(f_0+f_i)$. The model is periodic in f_0 with period 1 and has symmetric reflection about $f_0=\frac{1}{2}$ in the interval $[0,1]$. Thus we will restrict our analysis to values of f_0 within the interval $[0,\frac{1}{2}]$.

When writing Eq. (1) we have made a convenient gauge choice: We consider that the vector potential is parallel to the long axis of the ladder, and takes opposite values on the upper and lower branches (see Fig. 1). In this gauge f_0 and f_i are trivially related to the line integrals of the vector potential $\vec{a}$ through a link of the ladder:

$$a_{\alpha\beta}=\frac{2\pi}{\Phi_0}\int_\alpha^\beta \vec{a}\,d\vec{l}=\epsilon\pi(f_0+f_i),$$

where $\epsilon=+1$ (-1) for upper (lower) links in the ladder and $\epsilon=0$ for vertical links.

J_α $(\alpha=x,y)$, the Josephson coupling energy, is related to the critical current through the junction, $I_{c\alpha}$, by $J_\alpha=I_{c\alpha}\Phi_0/(2\pi)$. The inductance matrix of the array, L, is defined as

$$L_{ij}=\frac{\Phi_0}{I_{cx}}\frac{1}{8\pi^2\lambda_\perp}\Lambda_{ij}, \quad (2)$$

where Λ_{ij} is an adimensional matrix containing just geometrical coefficients (see the Appendix). $\lambda_\perp$ is the penetration depth, defined as in Ref. 8,

$$\lambda_\perp=\frac{1}{4\pi^2}\frac{\Phi_0^2}{\mu_0 J_x a}, \quad (3)$$

a being the lattice spacing.

It can be seen that the configurations which minimize Hamiltonian (1) comply with $\theta_i+\theta_i'=\text{const}$. Fixing this constant equal to 0 and normalizing by J_x in order to work with adimensional quantities we get

$$H=-\sum_i\left[2\cos(\theta_i-\theta_{i+1}-\pi f_0-\pi f_i)+\frac{J_y}{J_x}\cos(2\theta_i)\right] + \frac{\Phi_0^2}{2J_x}\sum_{ij} f_i L_{ij}^{-1} f_j , \quad (4)$$

where the quotient J_y/J_x defines the anisotropy of the ladder. To solve the ground-state phase diagram we will restrict our analysis to expression (4).

We consider here three approximations to the inductance matrix: The simplest model (case A) assumes a diagonal inductance matrix. In this case, the flux induced in a given plaquette only depends on the mesh current in the same plaquette. The next step in complexity, case B includes also nearest-neighbor inductances for the couplings between cells. Then, we assume $L_{ij}^{-1}=\tilde{L}\,\delta_{ij}+\tilde{M}\,\delta_{ij\pm1}$. Case C considers the full-range inductance matrix. In the first case the term in Eqs. (1) and (4) giving an account of the magnetic energy becomes

$$H_{\mathrm{magn}}=\sum_i d_K f_i^2 \quad \text{with} \quad d_K=8\pi^3\lambda_\perp(\Lambda^{-1})_{00}. \qquad (5)$$

In case B,

$$H_{\mathrm{magn}}=\sum_i d_K f_i^2+\sum_i \alpha d_K f_i(f_{i-1}+f_{i+1}). \qquad (6)$$

In the system under simulation (we consider square cells; currents are supposed to flow within a cylinder of length a and ratio $0.005a$) $d_K\approx 6.8\lambda_\perp$ and $\alpha=\widetilde{M}/\widetilde{L}\simeq 0.21355$.

We have used different methods to solve the problem. In the cases A and B it is possible to do it using an effective potential method properly adapted to study our model,[9] which is numerically equivalent to a 1D system with just next-nearest-neighbor interactions. The effective potential method is an efficient method to study the ground-state configurations of such kind of systems in the thermodynamic limit. This method is based on the computation of certain functions, the effective potentials, which contain all the relevant information on the relaxation of local fluctuations to the ground-state configurations.[10] A long computation time is required if one wants to obtain the phase diagram of the system with a high precision. This suggests the convenience of complementing the method with other procedures.

Effective potentials can provide, within a reasonable amount of time, approximate solutions to the ground-state problem as a function of the external field, the anisotropy of the ladder, and the penetration depth. Starting from these guesses, one can obtain more precise results by applying standard root-finding methods (calculating stable solutions to $\partial H/\partial x_i=0$) or even dynamically (letting the approximate solution relax). We make note that root-finding methods require the use of Eq. (1) to describe the system since Eq. (4) is just an adequate expression when dealing with minimum energy configurations, which is a reduced subspace of the whole system. We have checked that the same results are obtained if one applies the effective potentials method with a high precision or if one combines it with any of the complementary procedures described above. By comparing the energy curves corresponding to different configurations one can determine the border of the tongues with different vortex densities.

Moreover, making use of these procedures one can study how a ground-state configuration modifies when the parameters vary. In this case, it is convenient to keep in mind that, in general, a vortex configuration is stable beyond the range of parameters in which it is the ground-state solution. There, root-finding methods are adequate, and they must be completed by doing the linear stability analysis of the solutions.

Model C involves the total flux matrix. Interactions between the variables extend to all the lattice and the problem cannot be tackled with the effective potentials method. In this case, we consider the results achieved in approximation B as guesses and let the system evolve dynamically and relax down to the equilibrium. Details about the dynamical algorithm are given elsewhere.[11]

III. RESULTS: GROUND-STATE PHASE DIAGRAM AND STABILITY ANALYSIS

Figure 2(a) shows the ground-state phase diagram in the case of infinite penetration depth[3] $\lambda_\perp$ (thus neglecting CIMF's). The different tongues are characterized by the vortex density ω. This quantity is directly related to the periodicity of the configuration: a value $\omega=p/q$ implies that relevant physical quantities — gauge-invariant phases differences, induced fluxes, etc. — are spatially periodic: For every q plaquette these quantities are exactly repeated. Here vortices are defined as usual. We make use of the well-known property of fluxoid quantization to define the vorticity n_p on any plaquette. The clockwise sum of the gauge-invariant phases (restricted to the interval $(-\pi,\pi]$) along the links of the cell gives $\Sigma_{\alpha\beta\in i}(\Theta_\alpha-\Theta_\beta-a_{\alpha\beta})=2\pi(n_p-f^{\mathrm{tot}})$. The vortex density ω is equal to the spatial average of n_p.

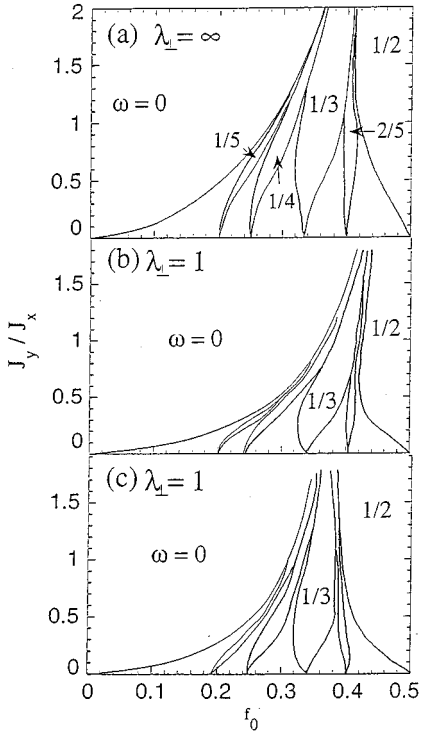

FIG. 2. Ground-state phase diagrams of the JJL obtained using the method of effective potentials. Each phase is defined by the value of ω and, for clarity, only a few of the transition lines are represented. (a) shows the results for the no-screening-field case (or $\lambda_\perp\to\infty$). (b) Phase diagram for a $\lambda_\perp=1.0$ ladder using approximation A (diagonal inductance matrix) to the calculation of the induced fluxes. (c) Phase diagram for a $\lambda_\perp=1.0$ ladder using approximation B (self plus nearest-neighbor inductances) to the calculation of the induced fluxes.

As mentioned in the Introduction, the vortex density as a function of the external field is a devil's staircase, with plateaus for every rational value of ω. Figures 2(b) and 2(c) show the phase diagram in the cases A and B, for a penetration depth $\lambda_\perp=1$, computed using the effective potentials method. Diagrams (b) and (c) are qualitatively similar to diagram (a). As one expects, the CIMF's tend to push the external magnetic field out of the array: As $\lambda_\perp$ decreases, the $\omega=0$ tongue grows. There is, however, a remarkable difference between these diagrams: While in case A all the tongues but the $\omega=0$ one compress, in case B the $\omega=\frac{1}{2}$ phase does not shrink, and the rest of the phases are com-

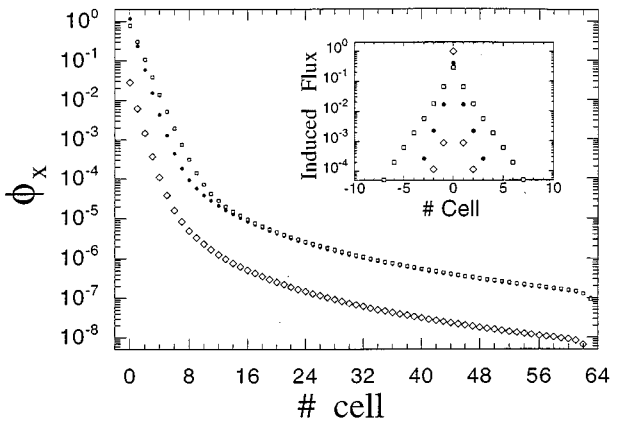

FIG. 3. Vortex shape as a function of the penetration depth $\lambda_\perp$ and the anisotropy. We consider an isotropic 128-cell ladder with just one vortex. The whole inductance matrix is used. $f_0=0$. The shape is symmetric, and we just draw the right half of the vortex (the origin of coordinates is the central plaquette of the ladder). The figure shows the gauge-invariant phase difference along the horizontal links belonging to the upper branch of the ladder. We compare the cases with $J_y=J_x$, $\lambda_\perp=1$ (black circles), $J_y=0.4J_x$, $\lambda_\perp=1$ (squares), and $J_y=J_x$, $\lambda_\perp=0.012$ (diamonds). The inset shows the induced flux around the central plaquette, in the same cases as before.

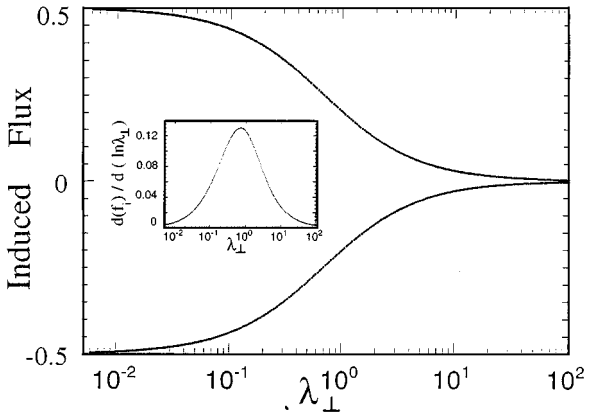

FIG. 4. Induced flux as a function of $\lambda_\perp$ for a configuration $\omega=\frac{1}{2}$, at $f_0=\frac{1}{2}$, $J_x=J_y$. We draw the flux through two plaquettes with vorticity 0 and 1, respectively. We consider the C case: whole inductance matrix. In the inset we show the derivative of the induced flux with respect to the logarithm of the penetration depth. We can distinguish three regions: the extreme limits $\lambda_\perp>4$ (the induced flux is $f_i=0+\delta/\lambda_\perp$) and $\lambda_\perp<0.12$ ($f_i=n_i-f_0+\delta\lambda_\perp$) and an intermediate region around $\lambda_\perp\sim0.7$, where the derivative is maximum.

pressed between these two. In short we will study carefully the limit of this behavior when $\lambda_\perp\to0$.

The effect of the CIMF's is to increase the critical field f_c up to which the $\omega=0$ configuration is the ground state. The devil's staircase is thus restricted to a narrower interval of values of the field.

The question arises whether CIMF's are able to change qualitatively the nature of the phase diagram. In other words, we want to check if for some $\lambda_\perp$ the array is able to expulse completely the external field and, consequently, this tongue occupies all the phase diagram. If this is not the case, is the devil's staircase structure preserved for all the values of $\lambda_\perp$?

In order to gain a more complete understanding of the properties of the model and, in particular, to throw light on the previously raised questions, it is interesting to study the dependence of the vortex characteristics on the different physical parameters. Such study is first carried out by considering commensurate phases with a low vortex density (e.g., $\omega=\frac{1}{128}$) in order to prevent vortex-vortex interaction effects. In particular, we are interested in studying the vortex extension. It is directly related to the distribution of the gauge-invariant phases around the vortex barycenter and depends on the values of J_y and $\lambda_\perp$ (see Fig. 3). In cells near the vortex center, the phase decays exponentially. This decay, as distance increases, becomes smoother; for large i (where i is the distance to the center), the phase is of the form ($\phi_i\sim i^{-3}$). Anisotropy affects the exponential part of the curve: A decrease of J_y implies a smoother exponential decay, while the long-distance behavior remains unchanged. Instead, varying $\lambda_\perp$ makes the whole curve shift. In cells far away enough from the center, the flux is negative and its absolute value is a decreasing function of the distance. The negative flux is due to the sign of the mutual inductance term (see the Appendix). This feature was already reported by Phillips *et al.*[2] As $\lambda_\perp$ decreases the vortex becomes more and more localized on its central plaquette and, in the $\lambda_\perp\to0$ limit, tends to identify with the fluxoid (the quantized magnitude defined above, which indicates the barycenter of the vortex). We can think of $\lambda_\perp$ as the radius of the vortex: $\lambda_\perp\to0$ implies that the vortex remains restricted just to the cell where $n_p=1$.

When no CIMF's are considered ($\lambda_\perp\to\infty$ limit) the total magnetic flux through a plaquette is just the external flux, which is constant along all the array. Thus, the flux distribution along the ladder is independent of the vorticity. Then, there is no flux quantization and the vortex density is not a flux quanta density but a fluxoid quanta density. On the contrary, the situation changes drastically when CIMF's are taken into account, the number and extension of vortices being directly connected to the distribution of the *induced* flux along the ladder. Let us consider the limit $\lambda_\perp\to0$ and the $\omega=0$ ground-state configuration; there, the currents tend to uniformly screen the external field (in every cell $f_i\to-f_0$). Thus, the array exhibits a behavior that resembles the Meissner effect: The external field is screened by the system and no field penetrates the array. For any other value of ω, the flux distribution is quite different. In the cells where the vorticity is equal to zero, the induced flux tends to cancel the external one, the total flux being equal to zero. In the cells where the vorticity is equal to 1, the induced flux $f_i\to(1-f_0)$, the total flux being equal to one flux quantum. Then, in the $\lambda_\perp\to0$ limit the fluxoid identifies with fluxon, and it is well localized in a cell of the array. This is illustrated in Fig. 4, where the dependence of the induced flux on $\lambda_\perp$ is shown both in cells with vorticities 0 and 1. We have chosen a configuration with $\omega=\frac{1}{2}$ and $f_0=\frac{1}{2}$, but the behavior is general: For other values of ω the fluxes in cells with zero vorticity depend on the distance to the nearest vortex, but this difference is of the order of $\lambda_\perp^2$ in the $\lambda_\perp\to0$ limit. We can distinguish three regions: For $\lambda_\perp>4$, $|f_i|\leqslant0.1f_0$,

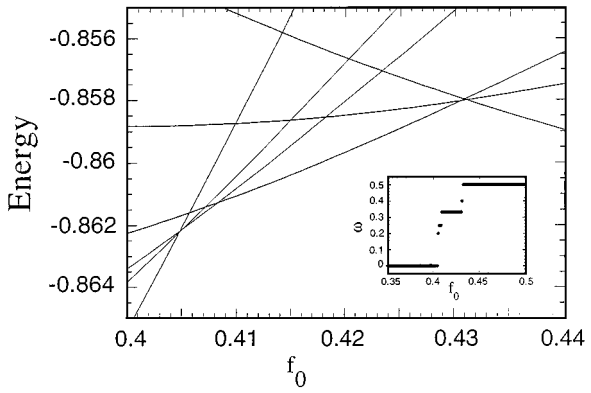

FIG. 5. Energies of different configurations as a function of frustration $[\epsilon_\omega(f_0)]$ for a penetration depth $\lambda_\perp=0.5$ in the case A. We study configurations w = 0, 1/5, 1/4, 1/3, 2/5, and 1/2 (in order of decreasing slope). We consider an isotropic ladder ($J_x=J_y$). The ground-state energy at each value of f_0 is given by the envelope of the curves. The inset shows the value of w corresponding to the minimum energy curve for each f_0.

and considering an infinite penetration depth is a justified approximation. On the other hand, for $\lambda_\perp<0.12$, we observe the low $\lambda_\perp$ behavior, $|f_i|>0.9(n_i-f_0)$, and screening fields are dominant. Between them there is an intermediate region, around $\lambda_\perp=0.7$ (where the derivative of the induced flux with respect to the logarithm of the penetration depth is maximum).

The description presented in the previous paragraph permits us to obtain some simple expressions for the energies of the different configurations for low values of $\lambda_\perp$. The Hamiltonian (1) consists of two components, corresponding to the Josephson and the magnetic energies. We have numerically checked that, as $\lambda_\perp\to 0$, the first term saturates before the magnetic one. Thus, for low enough $\lambda_\perp$, we can approximate the energy per plaquette by $E_p=-3+\Phi_0^2/2J_xN_p\ (n_i-f_0+\delta f_i)\ (L^{-1})_{ij}\ (n_j-f_0+\delta f_j)$, where $\delta f_i\sim O(\lambda_\perp)$, N_p is the total number of cells, and $n_i=0,1$ is the vorticity of cell i. Let us consider first case A in this approximation. The energy per cell of a configuration with $\omega=p/q$ is

$$E_p=-3+d_K\left(\frac{p}{q}(1-f_0)^2+\frac{q-p}{q}f_0^2\right).$$

As $f_0\in[0,\frac{1}{2}]$, $(1-f_0)\geqslant f_0$, and E_p is an increasing function of ω: For any $f_0=\frac{1}{2}$, $\omega_0<\omega_1$ implies $E(\omega_0)<E(\omega_1)$ and the configuration with $\omega=0$ is the ground state. If $f_0=\frac{1}{2}$, E_p, as previously defined, has the same value for all ω's. A second-order approximation in d_K is required. It is easily obtained that $E(\omega=\frac{1}{2};f_0=\frac{1}{2})<E(\omega=0;f_0=\frac{1}{2})$ [in particular, $E(\omega=0;f_0=\frac{1}{2})-E(\omega=\frac{1}{2};f_0=\frac{1}{2})=d_K^2/(6\pi^2J_y)$].

We remark that these results correspond to case A and an extreme limit ($\lambda_\perp\to 0$). Nevertheless, the devil's staircase is observable down to low values of $\lambda_\perp$ (we have checked this point even at $\lambda_\perp=0.012$). As an example, Fig. 5 shows the energy of stable configurations with different values of ω $(0,\frac{1}{2},\frac{1}{3},\frac{1}{4},\frac{1}{5},\frac{2}{5})$ as a function of the external field when $\lambda_\perp=0.5$. The energy of the ground-state staircase corresponds to the envelope of the curves; thus an approximation to the $\omega(f_0)$ function can be obtained from them.

Things change when one considers a more complete approximation to the inductance matrix (models B and C). In this case the $\omega=0$ phase does not fill the diagram at any value of $\lambda_\perp$ and other commensurate phases are clearly appreciated. Before performing a rigorous analysis, we present a plausibility argument in support of this statement. Let us begin by comparing $\omega=0$ and $\omega=\frac{1}{2}$ phases. In a $\omega=0$ configuration, the currents and flux are identical in all the cells. On the other hand, a configuration with $\omega=\frac{1}{2}$ exhibits a spatial periodicity with period $2a$; when $f_0=\frac{1}{2}$ the flux and currents on one cell are of the same module and the opposed sign with respect to those on the adjacent cells. This allows us to define an effective d_K for both configurations, so that the magnetic energy per cell is just $d_{K\,\mathrm{eff}}f_i^2$ (see the Appendix). In case B, $d_{K\mathrm{eff}}(\omega=0)=10.945\lambda_\perp$ and $d_{K\mathrm{eff}}(\omega=\frac{1}{2})=4.617\lambda_\perp$ while in case C, $d_{K\,\mathrm{eff}}(\omega=0)=11.176\lambda_\perp$ and $d_{K\,\mathrm{eff}}(\omega=\frac{1}{2})=4.638\lambda_\perp$. In general, for $w_0<w_1$ $d_{K\,\mathrm{eff}}(w_0)>d_{K\,\mathrm{eff}}(w_1)$, and thus $E(w_0;f_0=1/2)>E(w_1;f_0=1/2)$. As the energy is a continuous function of f_0 the previous inequality maintains for a range of f_0 values near $f_0=1/2$.

Moreover, it is possible to extend in a trivial way the argument previously developed for case A, and to calculate the energy per plaquette of any vortex distribution as a function of f_0. Note that a configuration with $\omega=p/q$ is described by a periodic spatial structure the basic subarray of which consists of q plaquettes containing p vortices. We can thus reduce the system to one with just q cells. In order to do that it is necessary to generalize the previous reckoning and to redefine the components of the matrix L in order to take into account the contribution of each of the infinite replicas of the basic subarray. Thus the inductance between two cells at distance j is given by $\hat{L}_j=\Sigma_n L_{0,j+nq}$, where $n=0,\pm1,\pm2,\ldots,\ j=0,\ldots,q-1$, and $L_{0,i}=L_{0,-i}$. In the limit $\lambda_\perp\to 0$ the induced flux in any cell is given by a vector $F\equiv\{f_af_bf_c\cdots\}$ with $f_i=(1-f_0+\delta f_i)$ or $(-f_0+\delta f_i)$ depending on the occupation number of the cell, n_i. Thus, the energy per plaquette, up to the first order in $\lambda_\perp$, is given by

$$E_p=-3+(\Phi_0^2/2J_xN_p)\,f_i(L^{-1})_{ij}f_j,$$

with $f_i=n_i-f_0$. We have computed this expression for a series of values of ω. By comparing the energies of the curves for different configurations we have obtained a devil's staircase; see Fig. 6. This figure corresponds to case C; in case B an analogous behavior is observed.

Hereafter, we will consider the response of the JJL to continuous variations of the external field. We will restrict our analysis to the study of the stability intervals of some simple commensurate phases which are the ground-state solution at some value of the parameters of the system [thus, we consider only ordered phases including just vortices (and no antivortices) and for which $0\leqslant\omega\leqslant\frac{1}{2}$]. Such a perspective, in the no-screening-field-effect limit, has been studied in Ref. 3 in order to characterize the dynamical approach to equilibrium, which has been shown to lead to slow relaxation. Here we will just focus on an important difference which appears when CIMF's are considered. Such study is carried out through a quasistatic computation of ordered

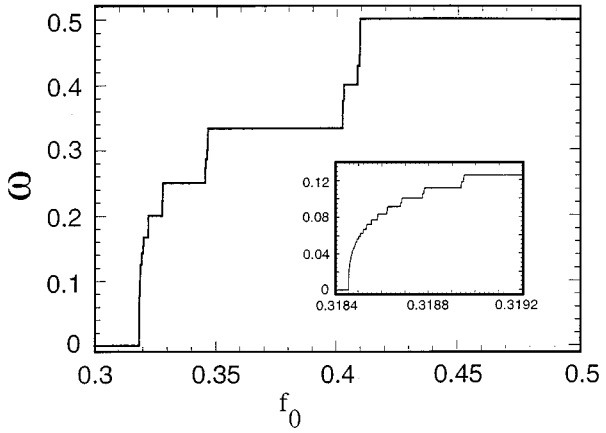

FIG. 6. Devil's staircase observed in case C in the limit $\lambda_\perp \to 0$ for an isotropic ladder, calculated as explained in the text.

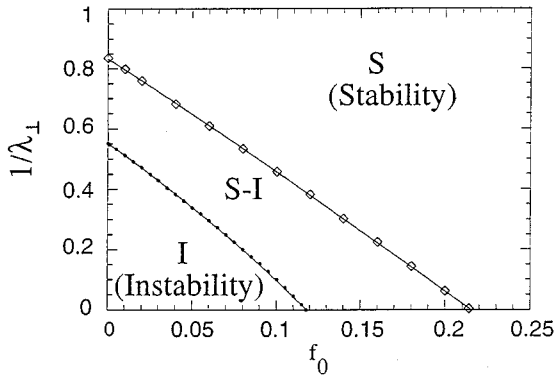

FIG. 7. Border between stability and instability regions in the parameter space for the extreme cases of one single vortex (black points) and $\omega = 1/2$ configuration (diamonds) in an isotropic ladder. In the first case we have considered a 128-cell ladder. We have checked that the curves fit to a quadratic function: $f_0 = \alpha(\beta + 1/[\lambda_{\perp c}(f_0)])*(1/[\lambda_{\perp c}(0)] - 1/[\lambda_{\perp c}(f_0)])$. $\lambda_{\perp c}(0)$ is the penetration depth below which a configuration is stable at $f_0 = 0$, and $\alpha\beta[1/\lambda_{\perp c}(0)] = f_c$, where f_c is the value of the frustration below which a configuration is no longer stable in the limit of no inductance ($\lambda_\perp \to \infty$). For a configuration with one single vortex, $f_c = 0.1175 \pm 0.000\,65$ and $\lambda_{\perp_c}(0) = 1.812 \pm 0.018$; in the $\omega = 1/2$ case, $f_c = 0.215 \pm 0.001$ and $\lambda_{\perp_c}(0) = 1.197 \pm 0.006$.

stable configurations [local minima of Hamiltonian (1)] with a determined vortex density, when the external field is slowly varied.

As previously mentioned, the range of stability of any vortex configuration (ω) is broader than the interval of the parameters in which it is the ground state. In general, there exists a critical value of the field for the stability of each phase: For $f_0 < f_c(\omega)$ the phase ω is no longer stable. The loss of stability when f_0 decreases occurs in this way: A decrease in the external field implies an increase in the supercurrent through the horizontal links in order to maintain the vortex density in the array. The instability of the state takes place when the supercurrent in one link reaches its maximum value. At this point any small change in the field cannot be sustained by an increase of the currents and the vortex structure becomes unstable, and the system relaxes to a new vortex configuration. That would be the process for the changes of vortex density when the external field is varied or when the thermal noise is high enough to produce a vortex to jump over the energy barrier of the metastable phase and then the system approaches to some other more stable phase.

In the limit of neglecting screening effects[3] $f_c(\omega) > 0$ for all $\omega \neq 0$, and thus when $f_0 = 0$ only the $\omega = 0$ phase is stable. The inclusion of CIMF's changes this situation. As $\lambda_\perp$ decreases the range of stability of a given phase enlarges. Moreover, for each configuration w there is a critical value for the penetration depth $\lambda_{\perp c}(\omega)$: If $\lambda_\perp < \lambda_{\perp c}(\omega)$, the phase is stable at every value of the external field. Let us consider the two extreme cases: The configuration containing one single vortex and the $\omega = 1/2$ phase. The repulsive character of the vortex-vortex interactions implies that the stability of the configuration containing a single vortex is a necessary condition for the stability of any phase with $0 < \omega \leqslant \frac{1}{2}$, so that the particular value of $\lambda_\perp$ at which stability of the configuration occurs $[\lambda_\perp^v(f_0)]$ is an upper bound for the stability of the phases with $0 < \omega \leqslant \frac{1}{2}$. On the other hand, stability of the $\omega = \frac{1}{2}$ phase ensures the stability of any other phase with $0 < \omega < \frac{1}{2}$, so that the particular value of $\lambda_\perp$ at which stability of the $\omega = \frac{1}{2}$ occurs $[\lambda_\perp^{1/2}(f_0)]$ is a lower bound for the stability of the phases with $0 < \omega < \frac{1}{2}$. Thus, $\lambda_{\perp c}^{1/2}(f_0) \leqslant \lambda_{\perp c}^{\omega_i}(f_0) \leqslant \lambda_{\perp c}^{v}(f_0)$. Figure 7 shows the regions of stability of the vortex configurations. For values of the parameters above the curves (region S), any vortex configuration is stable. In region S-I, as we move towards the origin of coordinates, the different states become unstable (in the order of decreasing ω). In I the only stable configuration is that with $\omega = 0$. Looking again at the supercurrents in the array, we see that as $\lambda_\perp$ decreases the gauge-invariant phase differences of the metastable configurations approach to zero and thus the supercurrents are lower, rendering the phase more stable.

IV. DISCUSSION

In Sec. III we have presented the phase diagram of a Josephson-junction ladder in the presence of screening magnetic field effects. Numerical results evidence the existence of a series of tongues labeled by the *mean vorticity* ω. Such magnitude exhibits a devil's staircase structure when the external field is varied.

When CIMF's are considered, the system presents a behavior that resembles the Meissner effect: The self-induced field tends to push the external field out of the array, causing the growing of the $\omega = 0$ tongue and the shrinking of the range of parameters where the devil's staircase is observed. We have compared the results of using different approximations when calculating the induced fluxes. If only the self-inductance term is considered, for a value of $\lambda_\perp$ low enough the $\omega = 0$ phase occupies all the phase diagram except for a tiny region near the $f_0 = \frac{1}{2}$ line. However, states with inserted fluxons are stable and, moreover, their range of stability increases as $\lambda_\perp$ decreases. Instead, if one takes into account the whole inductance matrix, the critical field for the $\omega = 0$ phase (the frustration above which the configuration is no more the ground state) remains lower than $\frac{1}{2}$ for all the values of the penetration depth. Thus commensurate phases with

vortices are always clearly visible in the phase diagram.

The three approximations made: A (self-inductance), B (self-inductance plus nearest-neighbor mutual inductance terms), and C (full-inductance matrix) correspond to different distributions of the relative weights of the inductance matrix components. We remark that these distributions are a function of the geometry of the currents flowing in the array (see the Appendix). Let us consider the case in which currents flow inside cylindric tubes of radius r and length equal to the lattice spacing a (the qualitative conclusions can be extended to any kind of cross section). If $r \ll a$, $\Lambda_{i,i} > |\Lambda_{i,i+1}| \gg |\Lambda_{i,i+j}|$ $(j>1)$ and approximation B (considering just the self-inductance plus the nearest-neighbor terms in Λ) is justified. As r increases, the terms $\Lambda_{i,i+j}$ $(j>1)$ also increase, but are yet too small. They give just small corrections to the final results. In a narrow range of r values around $r \sim 0.25$ the dominant contribution to the inductance is the self-term (and case A is a good zeroth-order approximation). Finally, for greater r, $|\Lambda_{i,i+j}|/\Lambda_{i,i}$ cannot be neglected and considering the whole inductance matrix is compulsory.

This behavior (the existence of an infinite set of ground states as the parameters vary which show a devil's staircase structure) is characteristic of a broad class of spatially modulated structures with convex interparticle interactions. In the limit of neglecting screening field effects ($\lambda_\perp \to \infty$) it is well established the equivalence, regarding the ground-state problem, of Hamiltonian (1) with a one-dimensional XY model with anisotropy and the ground-state problem of the system is equivalent to the one of a Frenkel-Kontorova model with convex interparticle interaction, which allows for applying the Aubry theory for this class of models.

However, and despite the qualitatively similar behavior shown by our simulations, the inclusion of CIMF's renders it difficult to establish any equivalence between model (1) and the 1D models named above. This point is beyond the scope of this paper and remains as an open question deserving future research.

The introduction of the CIMF's allows us to study the continuous variation of the system from the full penetration of the external field ($\lambda_\perp \to \infty$, $\Phi_i^{\rm tot} = f_0$, for $\lambda_\perp \geqslant 4$) limit to the case of an array where all magnetic flux, in the first order of $\lambda_\perp$, appears quantized [$\Phi_i^{\rm tot} = 0$ or $1 + O(\lambda_\perp)$], for $\lambda_\perp \leqslant 0.12$. This transition is reflected in Fig. 4.

An appealing question is that of the behavior — analysis of the robustness and stability especially — of different metastable configurations of a system under the variations of the external parameters. It provides information on the energy landscape of a system and other properties of the phase space which can determine interesting situations such as a constrained dynamics or slow relaxation processes. The inclusion of the CIMF's enlarges the stability range of the vortex configurations, as we have explicitly shown in the extreme cases of one single vortex and a $\omega = \frac{1}{2}$ phase.

Quite recently Hwang, Ryu, and Stroud[14] have extended the results on the ground-state properties of the Josephson-junction ladders in the large penetration depth limit, to treat the I-V characteristics of a ladder array. They found that when ''current is injected perpendicular to the ladder edges, the critical current is unchanged from its $f = 0$ value up to a penetration field of $f_{c1} \simeq 0.12$ flux quanta per plaquette.'' This result can be easily understood from the considerations on the stability of the one-vortex configuration we have made above. At low values of the external field the ground-state phase configuration of a bidimensional square Josephson-junction array has a vortex density different from zero and the existence of vortices produces a critical current lower than that of the $\omega = 0$ phase. In the ladder, however, the situation is quite different: At low values of f the ground state in the ladder is the $\omega = 0$ phase and, moreover, as we have described above, the configuration with just one vortex is unstable and the $\omega = 0$ phase is the only stable attractor for arbitrary initial phase configurations. Consequently, at low values of the external field the critical current of the ladder is expected not to change, since it depends on the vortex density. However, we have shown that the critical value of the field for the stability of the one single-vortex configuration is $f_c^v = 0.1175 \pm 0.000\,65$ for an isotropic ladder. For values of the field above f_c^v different vortex configurations are stable; thus, arbitrary initial phase configurations generically relax to different possible metastable configurations, which can be described as irregular arrays of vortices. In that situation the critical current is essentially associated with the depinning transition of these vortex phases, which occurs at a lower value of the external current. Hwang, Ryu, and Stroud give a value around 0.12, quite close to our prediction of $f_c^v = 0.1175 \pm 0.000\,65$.

As we have seen above, as $\lambda_\perp$ decreases, the value of f_c^v also decreases, vanishing at $\lambda_\perp = 1.812 \pm 0.018$. Then, the diagram of stability (Fig. 7) allows us to make the following conjecture on the behavior of the critical current of the Josephson-junction ladder when current-induced magnetic fields are taken into account: As the penetration depth decreases, the range of values of the external field for which the critical current remains unchanged also decreases and it vanishes when $\lambda_\perp = 1.812 \pm 0.018$. This conjecture is based on the natural association between the critical current of the ladder and the stability of the one-vortex configuration.

ACKNOWLEDGMENTS

We are indebted to C. Giovannella, F. Falo, and L. M. Floría for many useful discussions on this and related subjects. J.J.M. thanks C. Giovannella, J. C. Ciria, and the Dipartimento di Fisica in the Università di Roma Tor Vergata for their hospitality and making their facilities available to him. J.C.C. was supported by a grant from MEC (Spain). J.J.M. was supported by a grant from from MEC (Spain), the Project No. PB92-0361 (DGICYT) and European Union (NETWORK on Nonlinear Approach to Coherent and Fluctuating Processes in Condensed Matter and Optical Physics, Grant No. ERBCHRXCT930331).

APPENDIX: THE INDUCTANCE MATRIX

The L matrix is obtained in the following form: We have applied the Biot-Savart law in order to calculate the magnetic field induced on a link by all the currents circulating in the array. We thus obtain

$$\int_\alpha^\beta \vec{a}^{\rm ind} d\vec{l} = \sum_{\gamma\delta} FF_{\alpha\beta;\gamma\delta} I_{\gamma\delta}, \tag{A1}$$

where FF is the form matrix, which depends on the geometry of the array, and $I_{\alpha\beta}$ the total current passing through link $\alpha\beta$. If the links $\alpha\beta$ and $\gamma\delta$ are perpendicular we take $FF_{\alpha\beta;\gamma\delta}=0$.

The self-inductance term $FF_{\alpha\beta;\alpha\beta}$ depends strongly on the form of the current. If, for example, it is supposed to flow within a tube of length l with circular cross section of radius r it is given by

$$FF_{\alpha\beta;\alpha\beta}=2l\left[\ln\left(\frac{2l}{r}\right)-\frac{3}{4}\right]. \tag{A2}$$

If l is measured in meters, FF is given in 10^{-1} H.

Instead, the mutual inductances between different links are sensibly the same as that of the filaments through the centers of their cross sections, even when the links are very close. In particular, in the case of cylindric currents, the mutual inductances are absolutely independent from the radius.

In order to express Eq. (A1) as a function of adimensional quantities we introduce $ff=(4\pi/\mu_0 a)FF$, thus obtaining

$$a^{\rm ind}_{\alpha\beta}=\frac{2\pi}{\Phi_0}\int_\alpha^\beta \vec{a}^{\rm ind}d\vec{l}=\frac{1}{4\pi\lambda_\perp}\sum_{\gamma\delta} ff_{\alpha\beta;\gamma\delta}i_{\gamma\delta}, \tag{A3}$$

where currents are normalized to the critical current of the link I_c (in the case of an anisotropic ladder, where $I_x=I_y$, we take I_c as I_{cx}). $\lambda_\perp$ is the penetration depth; see Eq. (3).

It is easy to obtain an equivalent description of the self-field effect in terms of the mesh currents and the magnetic flux, as required in Eq. (4). The magnetic flux on an i cell is given by

$$\Phi^{\rm ind}_i=\oint_i \vec{a}^{\rm ind}d\vec{l}=\frac{\Phi_0}{2\pi}\sum_{\alpha\beta\in i} a^{\rm ind}_{\alpha\beta}, \tag{A4}$$

where the sum is over the four links $\alpha\beta$ of cell i, and can be expressed by a linear equation of the form

$$\sum_{\alpha\beta\in i} a^{\rm ind}_{\alpha\beta}=A_{i;\alpha\beta}a^{\rm ind}_{\alpha\beta}. \tag{A5}$$

We have used greek and roman symbols to denote, respectively, links and cells.

On the other hand, also the mesh currents (i_i) are related to the link currents ($i_{\alpha\beta}$) through a linear operator

$$i_{\alpha\beta}=\sum_{\alpha\beta\in i} B_{\alpha\beta;i}i_i. \tag{A6}$$

Combining Eqs. (A3), (A4), (A5), and (A6) we obtain

$$\Phi^{\rm ind}_i=L_{ij}I_j, \quad L_{ij}=\frac{\Phi_0}{I_c}\frac{1}{8\pi^2\lambda_\perp}\Lambda_{ij}, \tag{A7}$$

$$\Lambda_{i;j}=\sum_{\alpha\beta}\sum_{\gamma\delta} A_{i;\alpha\beta}FF_{\alpha\beta;\gamma\delta}B_{\gamma\delta;j}.$$

The $\Lambda_{i;j}$ elements depend on the distance $|i-j|$ between the cells considered. The general properties of matrix $\Lambda_{i;j}$ are that Λ_{00} is positive, and $\Lambda_{i;j}<0$ for $i=j$; for two cells far away enough ($|i-j|\geqslant 10$) the mutual inductance is $|\Lambda_{ij}|\sim|i-j|^{-3}$, as calculated in Ref. 13.

In the following, we will consider that currents flow inside cylindric tubes with circular cross section of radius r. If currents are supposed to have a very small cross section (compared to the lattice spacing a), then $ff_{\alpha\beta;\alpha\beta}\gg ff_{\alpha\beta;\gamma\delta}$. Then it can be easily verified that $\Lambda_{ii}\sim 8\ln(1/r)$ and $\Lambda_{i,i+1}\sim -2\ln(1/r)$. The other terms $|\Lambda_{i,i+j}|_{(j>1)}\ll\Lambda_{ii}$ can be neglected. As the cross section increases, $ff_{\alpha\beta;\alpha\beta}$ becomes smaller while the rest of the ff's remain sensibly the same; $\Lambda_{i,i}$ decreases, $\Lambda_{i,i+1}$ increases and changes sign at $r\sim 0.24a$, and $\Lambda_{i,i+j}$ $(j>1)$ remain the same. There is a range of r values $r\in[0.2,\ 0.28]$ where $|\Lambda_{i,i}|>20|\Lambda_{i,j}|$ $(j=i)$.

Thus we can establish r ranges where the different approximations A, B, and C made in the paper are acceptable. If $r\ll a$, $\Lambda_{i,i}>|\Lambda_{i,i+1}|\gg|\Lambda_{i,i+j}|$ $(j>1)$ and approximation B (considering just the self-inductance plus the nearest-neighbor terms in Λ) is justified. As r increases, the terms $\Lambda_{i,i+j}$ $(j>1)$ also increase, but are yet too small. They give just small corrections to the final results. In a narrow range of r values around $r\sim 0.25$ the dominant contribution to the inductance is the self-term (and case A is a good zeroth-order approximation). Finally, for greater r $|\Lambda_{i,i+j}|/\Lambda_{i,i}$ cannot be neglected and considering the whole inductance matrix is compulsory.

In our calculations, we have considered square cells; for the study of case C we have considered an intermediate value of r [currents are supposed to flow within a cylinder of length a and ratio $0.005a$ (Ref. 12)]. In this case, $\Lambda_{0;0}=38.194$ and $\Lambda_{0;i}/\Lambda_{00}\equiv\{1,\ -0.203\,32,\ -0.004\,011\,8,\ -0.001\,057\,0,\ \ldots\}$.

We can now calculate the equivalent d_K in the case $f_0=\frac{1}{2}$ for the configurations $\omega=0$ and $\omega=\frac{1}{2}$. This can be easily made if one considers the spatial periodicity of the solutions. If $\omega=0$, all the cells in the array have the same flux and current; thus we can define an effective self-inductance matrix as

$$f_i=[L_{i;i}+2*(L_{i;i+1}+L_{i;i+2}+\ \ldots)]i_i=L_{\rm eff}i_i, \tag{A8}$$

where the factor of 2 is due to the sum of the contributions from the cells on the left and on the right. The terms $L_{ij}, i\neq j$ are negative and thus $L_{\rm eff}<L_{ii}$. Now $d_{K\,\rm eff}\ (\omega=0)=8\pi^3/L_{\rm eff}=11\,176\lambda_\perp$.

In an analogous way, one can calculate the value of $L_{\rm eff}$ for an $\omega=\frac{1}{2}$ solution: For $f_0=\frac{1}{2}$ the flux and the current in one cell have the same magnitude and the inverse sign of those in the adjacent plaquettes. Thus

$$f_i=[L_{i;i}+2*(-L_{i;i+1}+L_{i;i+2}-\ \ldots)]i_i=L_{\rm eff}i_i, \tag{A9}$$

where now $L_{\rm eff}>L_{ii}$ and $d_{K\,\rm eff}\ (\omega=\frac{1}{2})=8\pi^3/L_{\rm eff}=4\,638\lambda_\perp$.

[1] For a recent view on the state of the art, see, e.g., *Macroscopic Quantum Phenomena and Coherence in Superconducting Networks*, edited by C. Giovannella and M. Tinkham (World Scientific, Singapore, 1995).

[2] A. Majhofer, T. Wolf, and W. Dieterich, Phys. Rev. B **44**, 9634 (1991); D. Domínguez and J. V. José, Phys. Rev. Lett. **69**, 514 (1992); J. R. Phillips, H. S. J. van der Zant, J. White, and T. P. Orlando, Phys. Rev. B **47**, 5219 (1993); D. Dominguez and J. V. José, *ibid.* **53**, 11 692 (1996).

[3] J. J. Mazo, F. Falo, and L. M. Floría, Phys. Rev. B **52**, 10 433 (1995).

[4] C. Denniston and C. Tang, Phys. Rev. Lett. **75**, 3930 (1995).

[5] An extensive list of references on the Frenkel-Kontorova model can be found in L. M. Floría and J. J. Mazo, Adv. Phys. (to be published).

[6] S. Aubry, in *Structures et Inestabilités*, edited by C. Godreche (Editions de Physique, Les Ulis, France, 1985), pp. 73–194.

[7] Hamiltonian (1) is adequate in the classic regime, where charging effects are neglectible. Granato has studied the quantum ladder problem in E. Granato, in *Quantum Dynamics of Submicron Structures*, edited by H. A. Cerdeira, B. Kramer, and G. Schön (Kluwer Academic, Dordrecht, 1995), p. 627.

[8] T. P. Orlando, J. E. Mooij, and H. S. J. van der Zant, Phys. Rev. B **43**, 10 218 (1991).

[9] S. Marianer and L. M. Floría, Phys. Rev. B **38**, 12 054 (1988); L. M. Floría and R. B. Griffiths, Numer. Math. **55**, 565 (1989).

[10] R. B. Griffiths and W. Chou, Phys. Rev. Lett. **56**, 1929 (1986); W. Chou and R. B. Griffiths, Phys. Rev. B **34**, 6219 (1986); R. B. Griffiths, in *Fundamental Problems in Statistical Mechanics VII*, edited by H. van Beijeren (North-Holland, Amsterdam, 1990), pp. 69–110.

[11] J.C. Ciria and C. Giovannella, J. Phys. Condens. Matter (to be published).

[12] A. Nuvoli, A. Giannelli, J.C. Ciria, and C. Giovannella, Nuovo Cimento **16**, 2045 (1994).

[13] D. Domínguez and J. V. José, Int. J. Mod. Phys. B **8**, 3749 (1994).

[14] I. Hwang, S. Ryu, and D. Stroud, Phys. Rev. B **53**, R506 (1996).